Lead-free piezoelectric system $(Na_{0.5}Bi_{0.5})TiO_3$-$BaTiO_3$: Equilibrium structures and irreversible structural transformations driven by electric field and mechanical impact

Rohini Garg,[1] Badari Narayana Rao,[1] Anatoliy Senyshyn,[2] P. S. R. Krishna,[3] and Rajeev Ranjan[1,*]

[1]*Department of Materials Engineering, Indian Institute of Science Bangalore-560012, India*

[2]*Forschungsneutronenquelle Heinz Maier-Leibnitz (FRM II). Technische Universität München, Lichtenbergestrasse 1, D-85747 Garching b. München, Germany*

[3]*Solid State Physics Division, Bhabha Atomic Research Centre, Tromaby, Mumbai-400085, India*

(Received 22 January 2013; revised manuscript received 25 April 2013; published 8 July 2013)

The structure-property correlation in the lead-free piezoelectric $(1-x)(Na_{0.5}Bi_{0.5})TiO_3$-$(x)BaTiO_3$ has been systematically investigated in detail as a function of composition ($0 < x \leqslant 0.11$), temperature, electric field, and mechanical impact by Raman scattering, ferroelectric, piezoelectric measurement, x-ray, and neutron powder diffraction methods. Although x-ray diffraction study revealed three distinct composition ranges characterizing different structural features in the equilibrium state at room temperature: (i) monoclinic (Cc) + rhombohedral ($R3c$) for the precritical compositions, $0 \leqslant x \leqslant 0.05$, (ii) cubiclike for $0.06 \leqslant x \leqslant 0.0675$, and (iii) morphotropic phase boundary (MPB) like for $0.07 \leqslant x < 0.10$, Raman and neutron powder diffraction studies revealed identical symmetry for the cubiclike and the MPB compositions. The cubiclike structure undergoes irreversible phase separation by electric poling as well as by pure mechanical impact. This cubiclike phase exhibits relaxor ferroelectricity in its equilibrium state. The short coherence length (~50 Å) of the out-of-phase octahedral tilts does not allow the normal ferroelectric state to develop below the dipolar freezing temperature, forcing the system to remain in a dipolar glass state at room temperature. Electric poling helps the dipolar glass state to transform to a normal ferroelectric state with a concomitant enhancement in the correlation length of the out-of-phase octahedral tilt.

DOI: 10.1103/PhysRevB.88.014103 PACS number(s): 77.80.−e, 77.22.−d, 77.80.Jk, 77.84.Cg

I. INTRODUCTION

Among the piezoelectric ceramics $Pb(Zr_xTi_{1-x})O_3$ (PZT) is the most widely used material for the past five decades due to its excellent piezoelectric properties.[1] However, due to the toxicity of lead, efforts are being made to discover a lead-free alternative. The solid solution system $(1-x)(Na_{0.5}Bi_{0.5})TiO_3$ (NBT)-$(x)BaTiO_3$ (BT) has received considerable attention in the recent past due to its better piezoelectric properties near the morphotropic phase boundary (MPB) at $x = 0.06 - 0.07$.[2–19] Although there is unanimity with regard to the importance of MPB for achieving higher piezoelectric properties in ferroelectric systems, as has been demonstrated extensively in lead-based systems such as $Pb(Zr_xTi_{1-x})O_3$, $Pb(Mg_{1/3}Nb_{2/3})O_3$-$PbTiO_3$, and $Pb(Zn_{1/3}Nb_{2/3})O_3$-$PbTiO_3$,[20–25] the structure-property correlations in NBT-derived piezoelectrics is far from settled primarily due to the persistence of ambiguity with regard to the crystal structure of the parent compound NBT itself. Although recent studies have questioned the traditionally believed rhombohedral ($R3c$) structure of this compound,[26,27] the newly proposed average monoclinic (Cc) structure fails to explain the entire diffraction pattern satisfactorily.[28,29] For the NBT-BT system, some groups have even questioned the role of MPB for enhanced piezoelectric property.[6,11] These authors suggest that the enhanced piezoelectric response is obtained for pseudocubic compositions and not for those exhibiting coexistence of ferroelectric phases in its equilibrium state as in PZT. Even the reported equilibrium MPB range varies from one group to the other depending on the nature of the synthesis (chemical method or single crystal) and the characterization [x-ray diffraction (XRD), transmission electron microscopy (TEM), Raman] methods adopted.[2–13] Based on a Raman spectroscopy study, Eerd *et al.*[4] have reported a temperature-independent MPB of NBT-BT at $x = 0.05$ in the unpoled state that shifts to $x = 0.06$ after poling the specimen. Yao *et al.*[8] constructed a phase diagram of this system using a polarized light and piezoresponse force microscope and suggested the MPB to lie somewhere in the range of 0.055 to 0.06. Ma *et al.*[10] have suggested the existence of domains with $R3c$ symmetry for $0.04 \leqslant x \leqslant 0.06$, nanodomains of $P4bm$ symmetry for $0.06 \leqslant x \leqslant 0.11$ and large lamellar domains for $x \geqslant 0.11$ using a TEM study. Recently, Jo *et al.*[6] proposed two MPBs, the first located at $0.05 \leqslant x \leqslant 0.06$ and the other at $x \sim 0.11$. They suggested that the first boundary is associated with the changeover from $R3c$ symmetry to $R3m$, i.e., involving the untilting of the oxygen octahedra about its threefold axis, and the second boundary is associated with a change from rhombohedral ($R3m$) to tetragonal ($P4mm$) symmetry. In the poled state, MPB changes to a morphotropic phase region and extends from $x = 0.06$ to 0.11.

In recent years, electric field-dependent structural studies have gained increasing importance to understand the relationship between field-induced structural changes and its consequences on the piezoelectric properties of MPB systems.[30,31] Daniels *et al.*[14] have shown electric field-induced phase transformation from a pseudocubic to tetragonal symmetry for $x = 0.07$ by *in situ* high-resolution synchrotron XRD studies. *In situ* electric field neutron diffraction studies of $x = 0.06$ revealed a strong $a^-a^-a^-$ tilted structure with rhombohedral and tetragonal lattice distortions.[15] While there are sporadic reports by different groups about electric field-induced structural changes in this system, a comprehensive and systematic correlation between structure and piezoelectric properties is still lacking. One of the difficulties that is encountered with *in situ* electric field-induced structural change is related to the fact that such studies have to be done on dense solid

specimens that exhibit texture effects on poling. Diffraction data collected from such specimens are not conducive for accurate structural analysis. Very recently, Rao and Ranjan[32] have shown an irreversible monoclinic to rhombohedral structural transformation in NBT after application of a sufficient electric field. The retention of the irreversibly changed structure after removal of the electric field allows the pellets to be gently crushed and obtain a good-quality powder diffraction pattern for the sake of reliable crystal structure analysis. Following the success of this simple and effective strategy, we have adopted the same to unravel the details of the electric field-induced structural changes in the NBT-BT system and correlate it with the measured piezoelectric property across closely spaced compositions. The accurate structural analysis was possible due to the availability of a texture-free diffraction pattern, which unambiguously established the coexistence of two ferroelectric phases, monoclinic (Cc) + rhombohedral ($R3c$) for the precritical compositions in the equilibrium state and its irreversible transformation to a single-phase rhombohedral structure after sufficient poling. For the critical compositions exhibiting a cubiclike structure, both electric field and mechanical impact induces irreversible phase separation. The study also established an intimate correlation between the polar nanoregions and short coherence length of the out-of-phase octahedral tilt in the equilibrium state.

II. EXPERIMENTAL

Different compositions of $(1-x)$NBT-(x)BT were prepared by the conventional solid-state route by mixing stoichiometric ratios of dried Bi_2O_3, Na_2CO_3, TiO_2, and $BaCO_3$ in a planetary ball mill for 10 h in an acetone medium using zirconia vials and balls. The dried powder was calcined at 900 °C for 3 h in air and later pressed into pellets under uniaxial pressure of 250 MPa. The densities of the pellets were measured by the Archimedes method, and the average density was found to be ∼95%. Sintering was carried out at 1120 °C for 2 h in air. XRD study was carried out using Philips X'Pert High Score Plus powder diffractometer with Cu $K\alpha$ radiation. The mass absorption coefficient of NBT for Cu $K\alpha$ is 175.43 cm^2/g. This corresponds to a penetration depth of ∼9 μm, which is sufficiently larger than the average grain size (∼2 μm). The structural information obtained, therefore, represents the bulk specimen. The sintered pellets were painted with Ag paste for electrical contact. Electric poling was carried out by applying a dc field of 40–50 kV/cm for 15 min in silicone oil. Dielectric measurement were carried out on a Novocontrol impedance analyzer (Alpha-A). Piezoelectric measurements were carried with a Piezotest PM300. Polarization vs electric field loop was measured with a Radiant Precision Premier II loop tracer. To obtain powder diffraction patterns from the poled specimens (poled-crushed specimen), the poled pellets were manually polished to remove the silver electrode and later crushed into a fine powder in mortar and pestle. Raman spectroscopy was conducted using a Raman spectrometer (LabRAM HR800, Horiba Jobin Yvon) in backscattering geometry on unpoled-polished ceramics. The 514.5-nm line of an Ar laser was used as excitation source for the measurements. Neutron powder diffraction data were collected at the FRM-II, Germany (wavelength = 1.548 Å) and at Dhruva reactor, Bhabha Atomic Research Center, India (wavelength = 1.2443 Å). Structural analysis was carried out by Rietveld method using the FULLPROF package.[33]

III. RESULTS

A. Composition-induced structural instabilities at room temperature

Figure 1 shows the Raman spectra for various compositions of NBT-BT at room temperature. The Raman spectra of pure NBT is identical to what has been reported earlier by Kreisel *et al.*[34,35] While the peaks at 140 cm^{-1} and 275 cm^{-1} have been assigned to Na-O and Ti-O lattice vibrations, respectively,

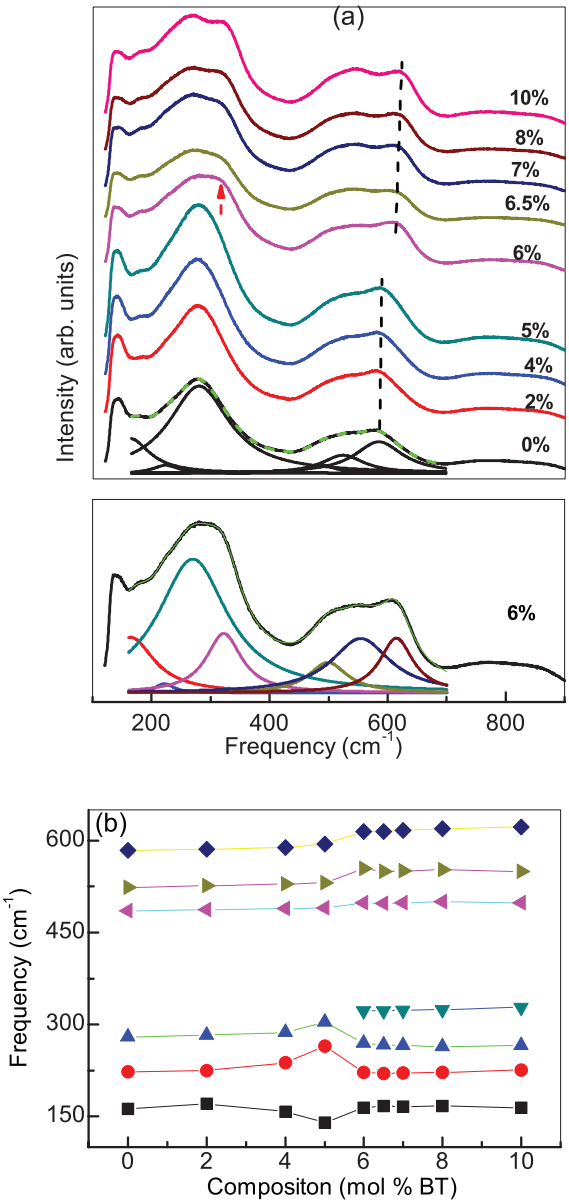

FIG. 1. (Color online) (a) Raman spectra for (1-x)NBT-(x)BT, $0 \leqslant x \leqslant 0.10$, at room temperature, the fit of multiple Lorentzian peaks are shown for $x = 0$ and 0.06. (b) Frequency shifts as determined by the multiple peak fitting of Lorentzian function to the spectra.

the three peaks in the range of 400–600 cm^{-1} have been attributed to rotations/vibrations of the oxygen octahedra. With increasing Ba-substitution, two important variations can be noted in the spectra: (i) weakening of mode close to 140 cm^{-1} and (ii) development of a flat top in the mode close to 275 cm^{-1}, which developed into a new peak at 320 cm^{-1} with increasing concentration in the composition range $0.06 \leqslant x \leqslant 0.10$. The composition variation of the mode frequencies obtained after deconvoluting the spectra with multiple Lorentzian functions is plotted in Fig. 1(b). Concomitant with the onset of the new mode at 320 cm^{-1}, the three octahedral modes near 500 cm^{-1} exhibit slight hardening for $x \geqslant 0.06$. Raman spectra therefore clearly confirm a composition-driven structural instability somewhere between $x = 0.05$ and $x = 0.06$.

Figure 2(a) shows the x-ray Bragg profiles of the pseudocubic $\{110\}_c$, $\{111\}_c$, and $\{200\}_c$ reflections of $(1-x)$NBT-(x)BT in the composition range of $0.05 \leqslant x \leqslant 0.10$. The

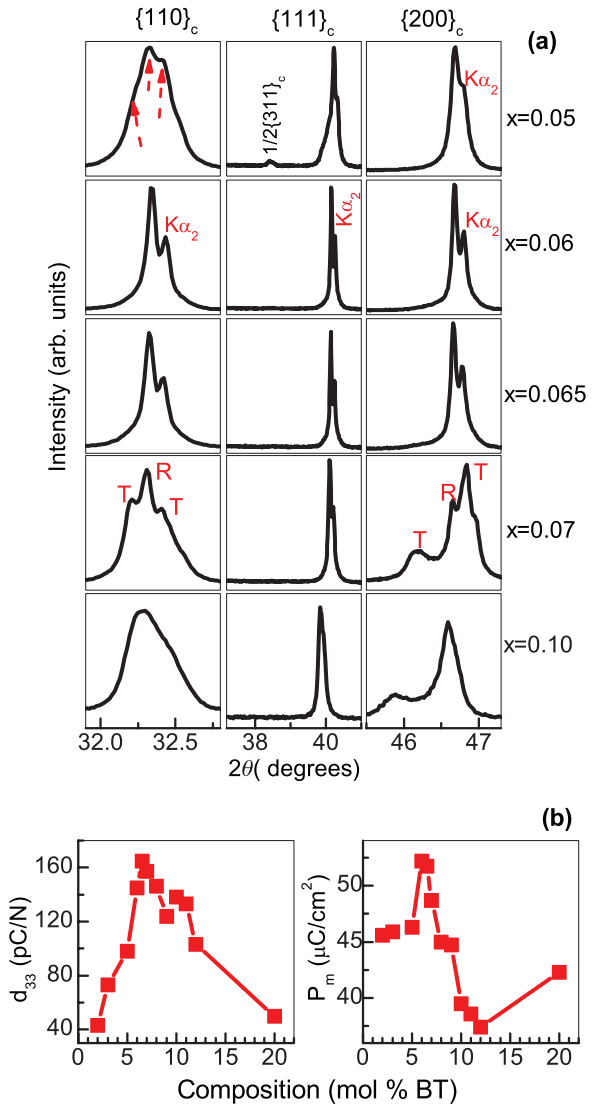

FIG. 2. (Color online) XRD pattern of selected Bragg peaks for $0.05 \leqslant x \leqslant 0.10$ (a) unpoled or annealed states (arrows indicate the splitting) and (b) composition dependence of piezoelectric coefficient (d_{33}) and maximum polarization (P_m) of $(1-x)$NBT-(x)BT.

Bragg profiles of $x = 0.05$ are similar to what has recently been reported for pure NBT.[29] In conformity with the Raman spectra, drastic changes in the x-ray powder diffraction pattern become visible when the Ba concentration changes from $x = 0.05$ to $x = 0.06$. Not only do the superlattice reflections characteristic of the out-of-phase octahedral tilt become invisible, but also all the Bragg profiles of $x = 0.06$ are singlet, suggesting a cubic-perovskite-like structure. Even a full width at half-maximum (FWHM) analysis of the Bragg peaks revealed their widths to be almost identical to the FWHM of the instrument. The cubiclike patterns were also found for two more nearby compositions, $x = 0.065$ and 0.0675. A sudden change in the XRD pattern occurs for $x = 0.07$. The triplet nature of the $\{200\}_c$ pseudocubic Bragg profiles of $x = 0.07$ can be explained on the basis coexistence of tetragonal and rhombohedral phases, a feature characteristic of an MPB system. Thus, while XRD suggests the existence of another phase boundary between $x = 0.06$ and $x = 0.07$, Raman spectra do not distinguish between $x = 0.06$ and $x = 0.07$. Figure 2(b) shows a composition variation of the longitudinal piezoelectric coefficient (d_{33}) and remnant polarization of NBT-BT. Both the properties exhibit similar trend with a maxima at $x = 0.065$. The d_{33} increases from ~ 98 pC/N for $x = 0.05$ to ~ 165 pC/N for $x = 0.065$ through 145 pC/N for $x = 0.06$. The anomalies in the properties are consistent with the structural instability observed at $x = 0.06$, observed both from the XRD and Raman studies. However, the fact that the cubiclike equilibrium structure exhibits as good a piezoelectric response as the composition exhibiting MPB appears counterintuitive. The issue was, however, resolved when the structures of the various compositions were analyzed after subjecting the specimens to electric poling (Sec. III D).

B. Structural analysis of the equilibrium precritical compositions $0 \leqslant x \leqslant 0.05$

As pointed out earlier, although the inadequacy of the rhombohedral structural model to fit the XRD patterns of pure NBT has been demonstrated by different groups,[26,27] the proposed monoclinic structure (Cc) cannot fit the x-ray powder diffraction patterns satisfactorily.[29] This has led to the speculation that NBT contains intrinsic structural disorder. An artificial cubic ($Pm\bar{3}m$) phase has been used by some groups in order to account for the features in the x-ray powder diffraction pattern that the single Cc structural model was not able to fit.[28,29] Since Rao and Ranjan have shown that a sufficiently poled specimen of pure NBT exhibits a pure rhombohedral structure,[32] the possibility of a rhombohedral structure cannot be completely ruled out. These observations suggest a likely scenario of the coexistence of ferroelectric phases even for the precritical compositions of NBT-BT. To understand the nature of the coexisting phases, we carried out a comparative fitting of the x-ray powder diffraction pattern of $x = 0.05$, the composition just below the threshold of the structural instability. We considered the following phase coexistence models: (i) pure Cc, (ii) $Cc + R3c$, (iii) $Cc + Pm\bar{3}m$, (iv) $Cc + P4bm$, and (v) $R3c + P4bm$. The consideration for the tetragonal $P4bm$ phase was based on recent electron diffraction studies that invariably reported the presence of

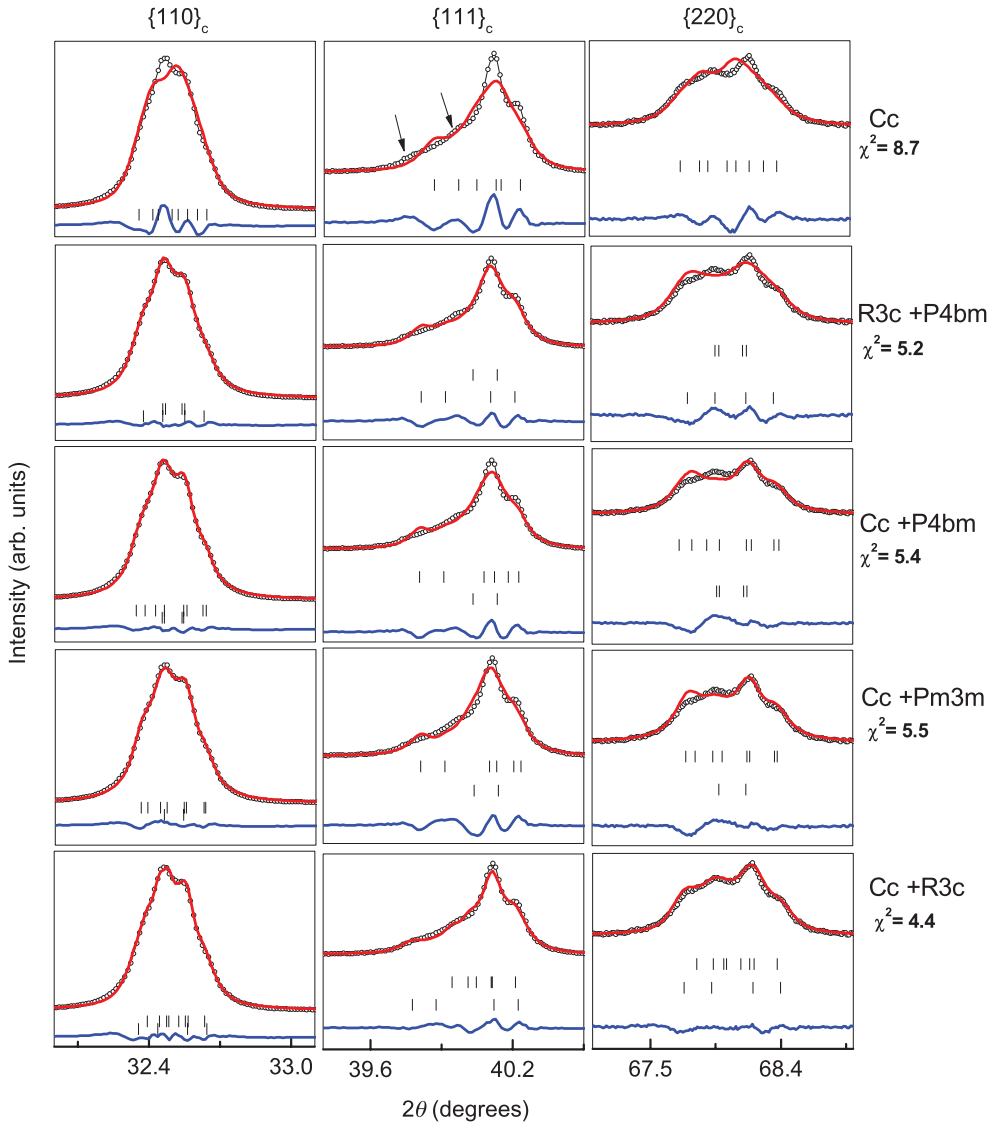

FIG. 3. (Color online) Observed (open circles), calculated (continuous line), and difference plots (continuous line at bottom), shown in a limited 2θ range for visual clarity, for $x = 0.05$ at room temperature after Rietveld refinement with the Cc, $R3c + P4bm$, $Cc + P4bm$, $Cc + Pm\bar{3}m$, and $Cc + R3c$ structural models. The upper and lower vertical bars correspond to the peak positions of $P4bm$ and $R3c$, Cc, and $P4bm$, Cc and $Pm\bar{3}m$, and Cc, and $R3c$, respectively.

this phase at room temperature along with the rhombohedral ($R3c$) phase.[36] The best-fit patterns with these models are shown in Fig. 3. As with the case reported for pure NBT, the single-phase monoclinic (Cc) model fits the Bragg profiles only in a crude average sense ($\chi^2 = 8.7$). As highlighted in Fig. 3, there are several regions in the diffraction pattern where remarkable discrepancies can be noted between the observed and the calculated patterns after the best possible fit with the Cc model. For example, while the observed $\{111\}_c$ shows the clear signature of three peaks (two shoulders on the left of the main peak, marked by arrows), the calculated profile shows only one peak in between the two small peaks. Although the $Cc + Pm\bar{3}m$ model fits the $\{110\}_c$ and $\{220\}_c$ profiles quite satisfactorily, it utterly fails to account for the first shoulder on the left of the main $\{111\}_c$. If this could be ignored, then the observed diffraction can be said to be fitted reasonably well by the $Cc + Pm\bar{3}m$ model, as has been reported earlier by Usher *et al.*[28] and Aksel *et al.*[29] The fit with $Cc + P4bm$ was no better than the $Cc + Pm\bar{3}m$ model. The $R3c + P4bm$ phase coexistence model, suggested invariably by all groups reporting the results of electron diffraction studies on this system,[37,38] could not produce the sufficient number of Bragg peaks to fit the profiles of the $\{220\}_c$ and $\{111\}_c$ reasonably well. The best fit, which could take into account all the peak positions most accurately, was found to be with the $Cc + R3c$ phase coexistence model. The refined parameters with the $Cc + R3c$ structural model are shown in Table I. The displacement parameters were fixed at one for all the atoms for the monoclinic phase as they were acquiring anomalous values without affecting the quality of the fit. In view of the field-dependent monoclinic to rhombohedral structural transition shown by Rao and Ranjan,[32] the $Cc + R3c$ model also seems to be the most plausible model for the precritical compositions of NBT-BT.

TABLE I. Refined structural parameters of annealed $x = 0.05$ with two-phase [monoclinic (Cc) and rhombohedral ($R3c$)] model and poled $x = 0.05$ with single-phase [rhombohedral ($R3c$)] structural model. The z coordinate of oxygen in the $R3c$ phase was fixed to avoid floating origin.

$x = 0.05$ (annealed)			Monoclinic (Cc) phase				Rhombohedral ($R3c$) phase			
a,b,c (Å)			9.5621(2)	5.4966(2)	5.5228(1)		5.4950(2)	5.4950(2)	13.5856(8)	
Na/Bi/Ba	x,y,z	B	0.0000	0.2500	0.0000	1(0)	0.0000	0.0000	0.2231(7)	2.2(1)
Ti	x,y,z	B	0.2543(6)	0.2538(1)	0.7809(3)	1(0)	0.0000	0.0000	−0.013(1)	1.1(5)
O1	x,y,z	B	−0.0114(51)	0.3153(24)	0.5357(59)	1(0)	0.122(2)	0.324(1)	0.08333	1(0)
O2	x,y,z	B	0.2427(7)	0.4954(8)	0.0494(3)	1(0)				
O3	x,y,z	B	0.2373(7)	0.0104(4)	0.0429(5)	1(0)				
β (angle°)			125.378(19)							
Phase fraction			60%				40%			
$x = 0.05$ (poled)			Rhombohedral ($R3c$) phase							
a,b,c (Å)							5.4963(1)	5.4963(1)	13.5834(3)	
Na/Bi/Ba	x,y,z	B					0.0000	0.0000	0.2235(4)	2.0(1)
Ti	x,y,z	B					0.0000	0.0000	−0.012(1)	0.74(8)
O1	x,y,z	B					0.1239(10)	0.3336(12)	0.08333	1(0)
Phase fraction							100%			

C. Structural analysis of the critical compositions $0.06 \leqslant x \leqslant 0.07$

1. XRD study

As shown above, the XRD patterns of the first few critical compositions in the narrow range $0.06 \leqslant x \leqslant 0.0675$ exhibit a cubiclike structure. Jo *et al.*[6] have speculated about the possibility of a $R3c$ to $R3m$ structural transition, involving the untilting of the oxygen octahedra, for such compositions. When we attempted to fit the XRD patterns of these compositions with any of the rhombohedral structural models ($R3c$ or $R3m$), the refinement was unstable and oscillatory. On the other hand, the refinement converged smoothly within a few cycles when the cubic ($Pm\bar{3}m$) model was chosen to fit the patterns. This confirmed that as far as the XRD patterns of these compositions are concerned, the Bragg peaks do not require a noncubic structure to account for their intensity and the profile shape. The cubic lattice parameters of these compositions $x = 0.06$, 0.065 were obtained as 3.9012 and 3.9023 Å, respectively. The increasing lattice parameters are in conformity with the fact that the ionic size of Ba (1.61 Å) is greater than the ionic size of Na (1.39 Å) and Bi (1.36 Å).[39]

The $\{200\}_c$ pseudocubic Bragg profile of $x = 0.07$ shows three peaks. In the past, compositions exhibiting such XRD peaks have been interpreted as showing a coexistence of tetragonal and rhombohedral phases.[6,9,10,15] Such compositions have accordingly been characterized as the MPB compositions. Since no superlattice reflections are visible in the XRD pattern, the tetragonal and the rhombohedral phases can be considered as $P4mm$ and $R3m$, respectively. Rietveld fitting with this model was able to explain the XRD pattern satisfactorily with a goodness of fit ($\chi^2 = 2.38$). The percentage phase fraction of the tetragonal and rhombohedral was found to be 60 and 40, respectively. Interestingly, however, we noted that the pseudocubic $\{111\}_c$ of $x = 0.07$ in Fig. 2(a) is strictly singlet. For a rhombohedrally distorted lattice, on the other hand, the $\{111\}_c$ should exhibit a doublet. This implies that, similar to $x = 0.06$, the rhombohedral lattice distortion is almost nonexistent in $x = 0.07$. In view of this, we also fitted the pattern of $x = 0.07$ with a tetragonal + cubic phase coexistence model and found a relatively better fit ($\chi^2 = 2.05$). This analysis suggests that the MPB compositions of the NBT-BT consist of a coexistence of tetragonal and cubiclike phases.

2. Neutron diffraction study

In the previous section, it was shown that while Raman spectra show only one phase boundary at $x = 0.06$, the XRD patterns suggest two phase boundaries at $x = 0.06$ and 0.07. The Raman spectra therefore do not make any distinction between $x = 0.06$ and 0.07. Since Raman modes are very sensitive to symmetry changes in crystalline materials, it may be argued that although $x = 0.07$ exhibits significant lattice distortion as compared to $x = 0.06$, symmetrywise they must be identical to each other. It may be noted that symmetries in perovskite structures are most often dictated by the relative positioning (tilt) of the adjacent oxygen octahedra with respect to each other. Such occurrences lead to the appearance of superlattice reflections in diffraction patterns. In the majority of cases, the superlattice reflections can be indexed on a doubled pseudocubic cell, suggesting that the octahedral tilts occur in a way that leads to doubling of the pseudocubic cell. Due to the low-scattering power of oxygen for x-rays, and if the magnitude of the tilt is small, it may sometimes be difficult to observe the superlattice reflections in XRD patterns. In such situations, reliable structural analysis can be done using neutron diffraction data only. Figure 4 shows neutron powder diffraction patterns of $x = 0.06$, 0.0675, and 0.10. Unlike the XRD patterns of these compositions (Fig. 2), the neutron diffraction patterns show additional weak superlattice reflections. To identify the superlattice reflections, we have marked all the possible peak positions in Fig. 4 along with their respective doubled pseudocubic index. It is evident that superlattice peaks in the pattern have indices as $\{310\}_{dc}$, $\{311\}_{dc}$, and $\{312\}_{dc}$. The subscript "dc" indicates a doubled pseudocubic cell. As shown by Glazer,[40,41] the superlattice

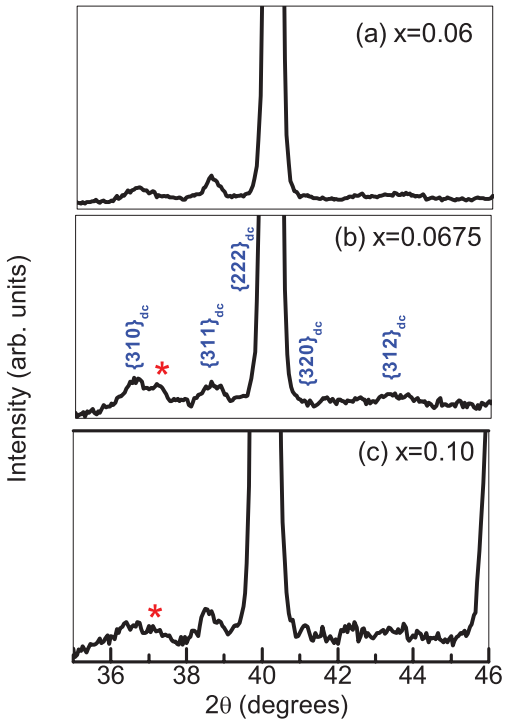

FIG. 4. (Color online) Neutron powder diffraction patterns of $(1-x)$NBT-(x)BT for $x =$ (a) 0.06, (b) 0.0675, and (c) 0.10. The indices are with respect to the doubled pseudocubic cell.

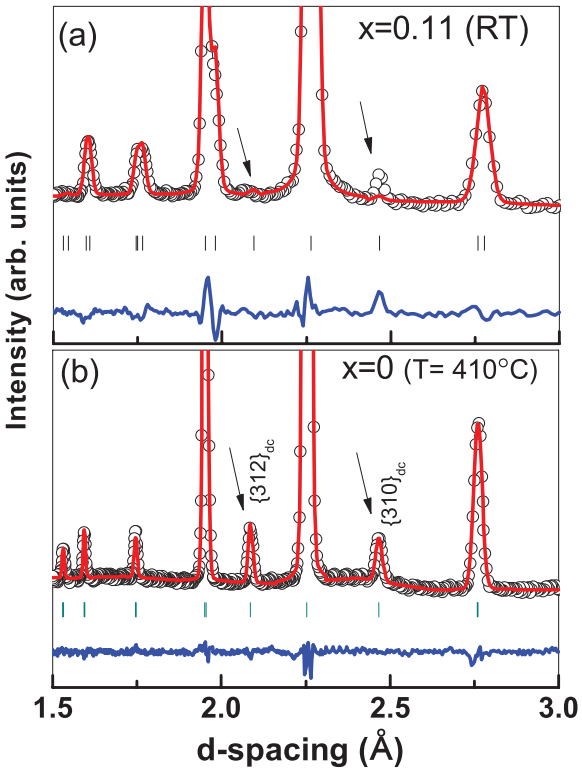

FIG. 5. (Color online) Rietveld fitted neutron powder diffraction pattern of (a) $x = 0.11$ and (b) NBT at 410 °C, both fitted with the $P4bm$ structure model. The two superlattice reflections, $1/2\{310\}_c$ and $\frac{1}{2}\{312\}_c$, characteristic of the tetragonal ($P4bm$) phase are shown in the lower figure.

reflections of odd-odd-odd (*ooo*) and odd-odd-even (*ooe*) types, respectively, arise from the out-of-phase and in-phase octahedral tilts, respectively, in the structure. Observation of both the types of superlattice reflections in electron diffraction patterns have led different groups to conclude about the coexistence of rhombohedral ($R3c$) and tetragonal ($P4bm$) phases in NBT-based systems.[3,10,15,16,19] In general the *ooo* superlattice peak is attributed to the $R3c$ phase and the *ooe* superlattice peaks to the $P4bm$ phase. The presence of the similar types of superlattice reflections in the patterns of $x = 0.06$, 0.0675, and 0.10, confirms that irrespective of the magnitude of the lattice distortions, the nature of the octahedral tilt is identical for all three compositions. This confirms the findings of the Raman study.

Since the XRD peaks of $x = 0.06$ and 0.0675 strictly suggest a cubic lattice parameter, the only way to reconcile the two-phase coexistence model for these compositions is to suggest that although both the structures have different symmetry, they have exactly the same cubiclike lattice parameter. In such a situation, there would be no misfit strain at the interphase boundary, and the coherency of the lattice can be strictly maintained. Since except for the superlattice reflections, which are different for the different phases, the main Bragg peaks are common to both the phases, it would not be possible to extract a reliable fraction of the two phases from Rietveld analysis—many different combinations of phase fractions can give the same fit with slightly altered structural parameters. We noted that neutron powder diffraction pattern of $x = 0.11$ showed only the *ooe* superlattice peaks. Rietveld fitting of this pattern was carried out using the $P4bm$ structural model. The outcome of this analysis, shown in Fig. 5, reveals that this structural model failed to account for the intensity of the $\{310\}_{dc}$ superlattice reflection. The $P4bm$ tetragonal phase was initially proposed by Jones *et al.*[42,43] to explain the *ooe*-type superlattice reflections in the neutron diffraction pattern of NBT in the temperature range of 300–540 °C. The asymmetric unit of the $P4bm$ structure consists of four atoms: Na/Bi/Ba at $(0, 0.5, 0.5+\delta_{Na/Bi})$, Ti at (0, 0, 0), oxygen O_1 at $(0, 0, 0.5+\delta_{Ti})$, and oxygen O_2 at $(0.25+\delta_{Oy}, 0.25-\delta_{Oy}, 0+\delta_{Oz})$. The intensity of the superlattice reflections is determined solely by the single parameter variable δ_{Oy}. From the simplicity of this structure model, it is highly unlikely that the poor fitting of the superlattice reflection could be due to inadequate refinement of the structural parameters. For sake of confidence, we used the same structure model to fit a neutron diffraction pattern of pure NBT at 410 °C. The very nice fit, shown in Fig. 5(b), validates the ability of this structural model to fit the high-temperature tetragonal phase of pure NBT and also proves that the remarkable misfit of the superlattice reflection in Fig. 5(a) is a genuine feature. What is intriguing to note is that the intensity of the peak near the $\{312\}_{dc}$ superlattice reflection is insignificantly small as compared to the intensity of the $\{310\}_{dc}$ superlattice peak in the pattern of $x = 0.11$. In sharp contrast to this, the intensity of the $\{312\}_{dc}$ is slightly higher than that of $\{310\}_{dc}$ in the 410 °C pattern of pure NBT [Fig. 5(b)]. This anomalous ratio is present for all the compositions in the range of $0.06 \leqslant x \leqslant 0.10$ (Fig. 4), and hence the $P4bm$ structure does not seem to be the correct structure of the tetragonal phase in the NBT-BT system. Within the Glazer's scheme of simple

octahedral tilts, apart from the $a^0a^0c^+$ tilt compatible with the $P4bm$ structure, other possible combinations of in-phase tilts are $a^0b^+b^+$, $a^+b^+c^+$, and $a^+a^+a^+$. They give rise to tetragonal ($I4/mmm$), orthorhombic ($Immm$), and cubic ($Im\bar{3}$) structures, respectively.[40,41] However, none of these models were able to fit the superlattice peaks satisfactorily.

A close inspection of the profile shape of the $\{310\}_{dc}$ superlattice reflection revealed another interesting feature that suggests that the structure of the tetragonal phase is far more complex. In the pattern of $x = 0.0675$, there is another weak peak immediately on the right side of $\{310\}_{dc}$. This additional weak peak, marked with * in Fig. 4(b), cannot not be indexed with respect to a doubled pseudocubic cell. In a later section (Sec. III E), we have shown that this additional peak originates from the same structure that gives other peaks in the pattern and is therefore not due to any unwanted impurity phase. The additional superlattice reflection therefore cannot be explained by any of the tilt systems in the Glazer's classification scheme.[40,41] The detailed analysis presented above therefore suggests a need to consider structural models beyond the scope of the simple octahedral tilts. In this paper we have not considered structural models based on higher modulations of the pseudocubic cell since such an analysis would require neutron powder diffraction data with much better counting statistics. However, following this analysis in the sections that follow, the tetragonal structure is described without any reference to the space group symmetry. This limitation does not come in the way of the analysis of the XRD patterns of the MPB compositions since, as mentioned above, the superlattice reflections are not visible, and for all practical purposes, the tetragonal peaks can be satisfactorily explained by a BT-like tetragonal ($P4mm$) structure.

D. Mechanical impact and electric field-induced irreversible structural transformations

It may be mentioned that since ferroelectric materials are also ferroelastic in nature, mere mechanical impact due to manual crushing of the specimen may cause structural/microstructural changes in the specimen. For investigating the structures of the equilibrium phases, it was, therefore, necessary to anneal powders obtained from the crushed pellets. All the structural analyses reported in the previous sections were, therefore, carried out on annealed powder specimens. Study of electric field-induced structural changes in ferroelectric materials is, in general, experimentally quite challenging and, in principle, can be carried out only by *in situ* experiments. However, the texture effect in the diffraction data obtained from the pellet under the *in situ* field most often severely limits the structural information one can obtain from such diffraction data. Interestingly, a way out of this problem was recently shown by Rao and Ranjan,[32] if the system exhibits irreversible changes after application of electric field, as in pure NBT. The poled pellets can subsequently be crushed gently to obtain powder, and the texture-free diffraction data collected from such poled-crushed powder would be suitable for extracting detailed structural information by Rietveld refinement.

Figure 6 shows the x-ray powder diffraction profiles of the pseudocubic peaks $\{110\}_c$,$\{111\}_c$, and $\{200\}_c$ of the unpoled, unpoled-crushed, and poled-crushed specimens of different compositions. A comparison of the profile shapes of the

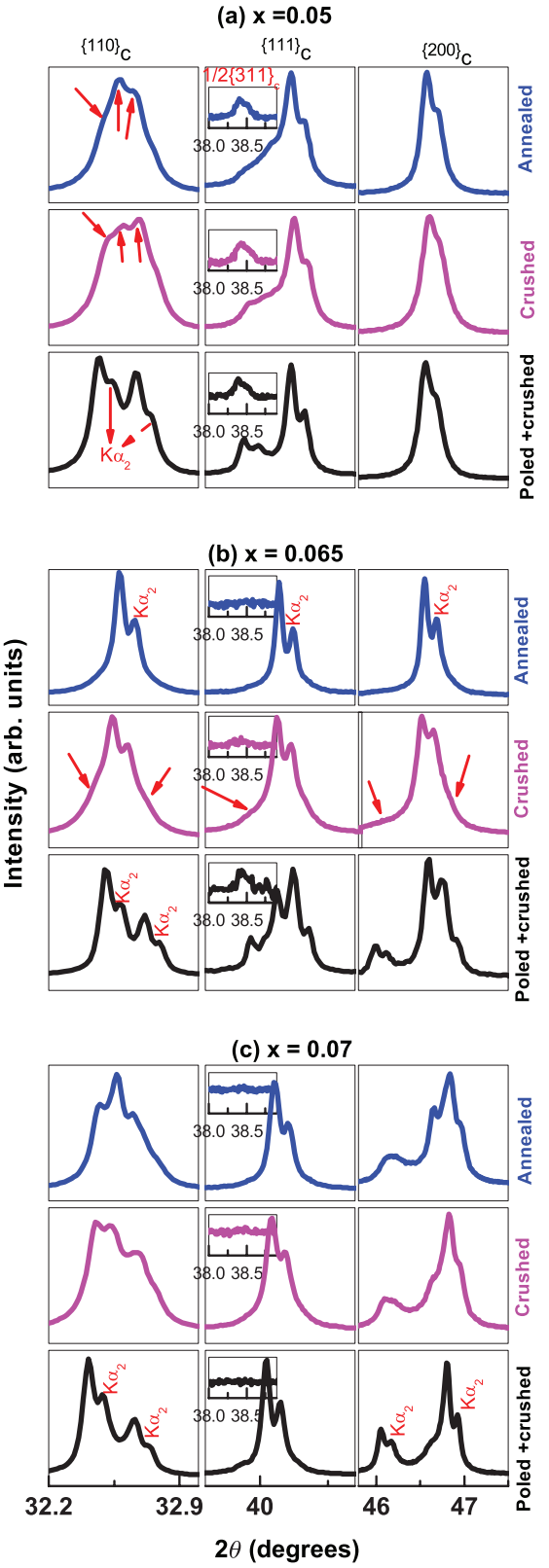

FIG. 6. (Color online) Comparison of annealed, crushed, and poled-crushed diffraction patterns of selected Bragg reflections for $0.05 \leqslant x \leqslant 0.07$. The insets shows the position of the $1/2(\{311\}_c$ superlattice reflection.

unpoled-crushed specimens with the corresponding profiles of the annealed specimens reveals the occurrence of impact-induced structural changes for all the compositions. The most significant change in the profile shape after manual crushing is revealed in the pseudocubic $\{110\}_c$ profile. For $x = 0.05$ and $x = 0.07$, the first two peaks of the triplet in the $\{110\}_c$ have become of comparable intensity after the mechanical impact. For $x = 0.065$, two humps, one on the left and another on the right [marked with arrows in Fig. 6(b)] become noticeable around each of the singlets. Similar alteration in the profile shapes of the pseudocubic $\{111\}_c$ profile becomes noticeable after crushing $x = 0.05$ and $x = 0.065$. It was possible to explain the structural changes induced by mechanical impact by one-to-one comparison of these profiles with the corresponding profiles obtained for the specimens that were sufficiently poled before crushing (poled-crushed specimens). These profiles are shown just below the profiles of the unpoled-crushed specimens in Fig. 6. Although in the first instance, it may appear that the overall Bragg profiles of the sufficiently poled-crushed specimens have no resemblance with those of the unpoled-crushed specimens, a closer look reveals that the additional peaks, or alteration in the relative intensity of the peaks noticeable in the unpoled-crushed specimens occur at the same 2θ positions where well-defined peaks become manifest in the poled-crushed pattern. This observation at once suggests that the nature of the irreversible structural changes induced by mechanical impact is similar to that induced by the electric poling. The only difference is that while the latter is able to alter the structural change to its possible limit, the former does it only partially.

1. *Irreversible transformations in the precritical compositions ($x \leqslant 0.05$)*

The diffraction patterns of the unpoled-crushed specimen of the precritical compositions were successfully fitted with the same $Cc + R3c$ phase coexistence model concluded for the annealed specimens (Sec. III B). Since the peaks corresponding to the different phases overlap considerably and also the number of peaks with strong intensity is limited in the XRD patterns, we carried out constrained refinement for the sake of obtaining consistency in the phase fraction. The atomic coordinates of the rhombohedral ($R3c$) and the monoclinic (Cc) phases were frozen at the values obtained for the annealed specimen (Table I). The fitted pattern obtained this way is shown in Fig. 7(b). It was found that the relative fractions of the $R3c$ changed from 40 to 82% after crushing. The pattern of the poled-crushed $x = 0.05$, on the other hand, could be successfully fitted with single-phase $R3c$ model, Fig. 7(a). It may be noted that the Bragg peaks of the electric field transformed pure rhombohedral phase are relatively sharp. This may be attributed to the decrease in the total volume fraction of the disordered regions around the Cc-$R3c$ interphase boundaries and also to the merger of small domains (present in the annealed state) to form larger domains on application of electric field. The rhombohedral structural parameters of the poled-crushed specimen are given in Table I. The close similarity of the structural parameters of the pure $R3c$ phase (poled crushed) and the $R3c$ phase coexisting with the Cc phase (annealed specimen) can be taken as independent proof in support of this phase coexistence model. The complex appearance of the observed diffraction patterns of the annealed as well as the unpoled-crushed specimens merely requires a certain fraction of the $R3c$ phase, without any change in the structural parameters, to fit the misfit regions in the XRD patterns, which were not accountable by the single-phase Cc model.

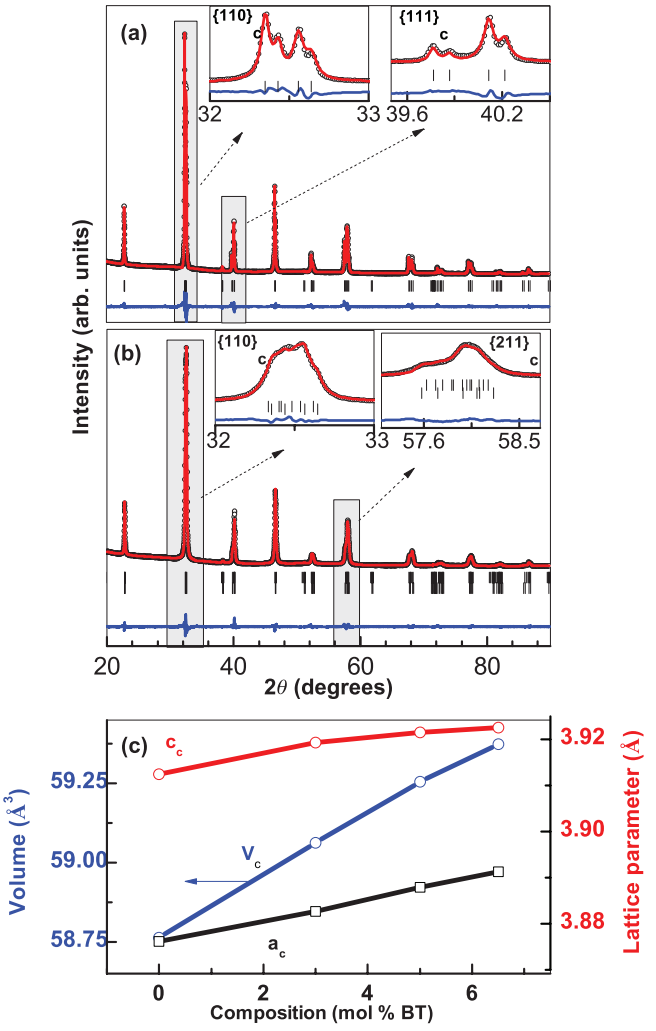

FIG. 7. (Color online) Rietveld refinement plot of (a) poled-crushed $x = 0.05$ with the structural model $R3c$ and (b) unpoled-crushed $x = 0.05$ with Cc + R3c structural model. The inset shows the limited 2θ range vertically magnified to exhibit the fits of the reflections' (c) volume and lattice parameter variation of poled-crushed sample with composition.

The transformation of $x = 0.05$ to a complete rhombohedral ($R3c$) phase after poling is similar to what has recently been demonstrated for pure NBT (Ref. 32) and confirms that the occurrence of field-induced monoclinic to rhombohedral irreversible transformation happens for all the precritical compositions ($x \leqslant 0.05$). The pseudocubic lattice parameters and cell volume of the rhombohedral phase obtained from sufficiently poled-crushed specimens of various compositions in the precritical range are shown in Fig. 7(c). The monotonously increasing volume with composition is consistent with the bigger ionic size of Ba^{+2} (1.61 Å) as compared to the size of the

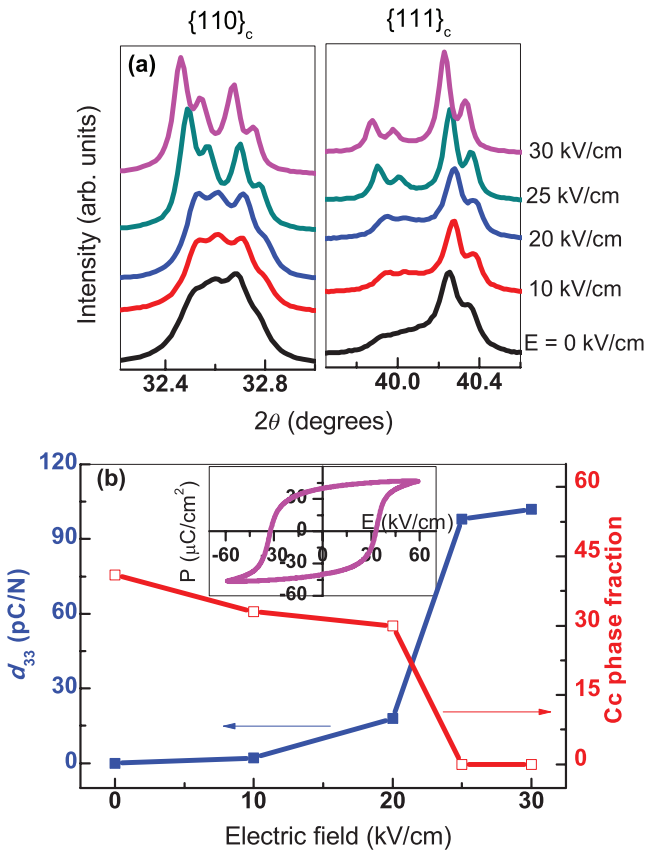

FIG. 8. (Color online) (a) XRD plots of $x = 0.05$ electrically poled at different electric fields. The applied electric fields are 0 kV/cm, 10 kV/cm, 20 kV/cm, 25 kV/cm, and 30 kV/cm from bottom (black color) to top (pink color), respectively. (b) The value of d_{33} and Cc phase fraction as a function of electric field. The inset shows the P-E loop for $x = 0.05$.

Na (1.39 Å) and Bi (1.36 Å).[39] We also studied the evolution of the pattern of the precritical composition ($x = 0.05$) as a function of electric field [Fig. 8(a)] and measured the longitudinal piezoelectric coefficient (d_{33}) of the pellet before crushing it for collecting the diffraction data. The relative decrease in the fraction of the monoclinic phase with the poling field is plotted along with d_{33} values of $x = 0.05$ [Fig. 8(b)]. It is evident from this plot that d_{33} saturates at the same field (25 kV/cm) at which the specimen has become completely rhombohedral. This field is close to the coercive field (~30 kV/cm) of the specimen [see inset of Fig. 8(b)]. This suggests that the energy cost of the Cc-$R3c$ transformation is more or less comparable to the energy needed to align the domains.

2. *Irreversible transformations in the MPB-like critical compositions ($x \geqslant 0.07$)*

For the MPB compositions, e.g., $x = 0.07$, perhaps guided by the common occurrence of tetragonal + rhombohedral phase coexistence in lead-based piezoelectrics, some groups have suggested the same coexistence model for the MPB compositions of the NBT-BT.[44,45] However, a close inspection of the profile shapes in Fig. 5(c) (annealed) did not reveal features of rhombohedral lattice distortion, such as splitting in the $\{111\}_c$ profile. In fact, Rietveld fit of unpoled-crushed $x =$

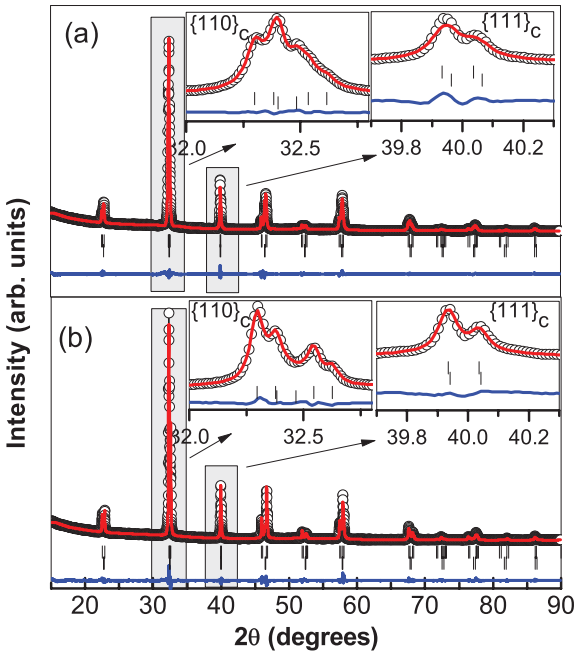

FIG. 9. (Color online) Observed (open circles), calculated (continuous line), and difference plot (with continuous line at bottom) for limited 2θ range for $x = 0.07$ after Rietveld refinement (a) in the unpoled state and (b) in the poled-crushed state with the $Pm\bar{3}m + P4mm$ structure model. The upper and lower vertical bars correspond to the peak positions of $Pm\bar{3}m$ and $P4mm$, respectively.

0.07 composition with rhombohedral + tetragonal ($T + R$) and cubic + tetragonal ($T + C$) resulted in identical fits with almost comparable χ^2 ($\chi^2_{T+R} = 5.00$ and $\chi^2_{T+C} = 5.45$). The fitted pattern of the annealed and poled-crushed patterns of $x = 0.07$ with $T + C$ phase model is shown in Figs. 9(a) and 9(b), respectively. Hence, it cannot be said with confidence that the MPB in the NBT-BT system is more or less akin to the MPB in lead-based systems. Our analysis suggests that MPB is a coexistence of the cubiclike and tetragonal phases. The intensity of the cubiclike peak slightly decreased after manual crushing. The decrease was found to be more for the poled-crushed specimen. Rietveld analysis suggested a decrease in the fraction of the cubic like phase from 38% to 31% after crushing and became ~25% in the poled-crushed specimen. Thus, unlike the precritical compositions, where poling led to complete transformation of the system from a two-phase ($Cc + R3c$) state to a single-phase ($R3c$) state, it retains the phase coexistence character of the MPB compositions. It is obvious from this study that the effect of poling on the equilibrium MPB compositions is to irreversibly increase the tetragonal fraction and decrease the cubiclike/rhombohedral phase. A continuity of this phenomenon will lead to the vanishing of MPB for higher compositions since poling would completely suppress the weak cubiclike peaks and make the system completely tetragonal, as has been reported by Picht *et al.*[9]

3. *Irreversible transformations in the cubiclike critical compositions ($0.06 \leqslant x \leqslant 0.0675$)*

As evident from Fig. 6, the most profound effect of mechanical impact and electric poling on the diffraction

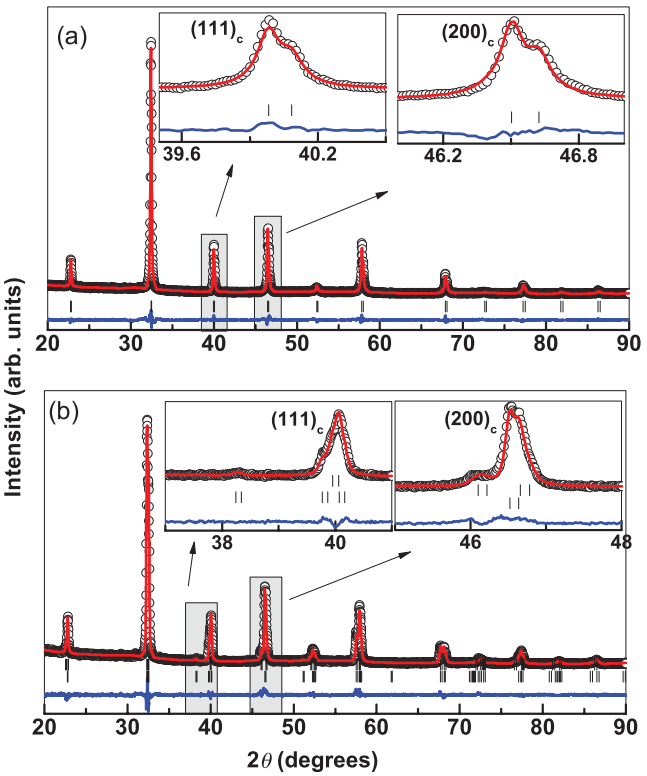

FIG. 10. (Color online) Observed (open circles), calculated (continuous line), and difference plot (with continuous line at bottom) for limited 2θ range for $x = 0.065$ after Rietveld refinement (a) in the unpoled state with $Pm\bar{3}m$ and (b) in the poled-crushed state with the $R3c + P4mm$ structure model, respectively.

pattern occurs for the compositions exhibiting a cubiclike phase in the equilibrium state (annealed specimen). Rietveld fit of the annealed specimen of $x = 0.065$ with a cubic ($Pm\bar{3}m$) structural model is shown in Fig. 10(a). The nice fit to the profile $\{111\}_c$ and $\{200\}_c$, shown in the inset, confirmed the absence of measurable lattice distortion (rhombohedral or tetragonal). As evident from the Bragg profiles of the poled-crushed specimen of this composition [Fig. 5(b)], all the singlet peaks split into multiple peaks. While the doublet nature of the $\{110\}_c$ and $\{200\}_c$ suggests the presence of a dominant tetragonal phase, the three peaks in $\{111\}_c$ correspond to a doublet of the rhombohedral phase and one singlet of the tetragonal phase. More interestingly, the $1/2\{311\}_c$ superlattice reflection (shown in the insets of the middle column of Fig. 6) characteristic of the rhombohedral ($R3c$) phase, which was not visible in the annealed state, becomes visible in the poled-crushed pattern. This is a clear evidence of a significant increase in the out-of-phase tilt angle in the phase-separated rhombohedral structure. Rietveld fitting of the pattern with a tetragonal + rhombohedral phase coexistence model is shown in Fig. 10(b), and the refined structural parameters are given in Table II. We may note that since the superlattice reflections corresponding to the tetragonal phase are not visible in the XRD pattern, we used the BT-type tetragonal structure ($P4mm$) in our structure analysis. For the specimen that was merely crushed without poling, noticeable humps appear on either side of the cubiclike peaks [Fig. 6(b), crushed]. These humps, marked with arrows, occur at almost the same positions where the tetragonal and rhombohedral peaks appear in the poled pattern. Excess intensity above the background near the $1/2\{311\}_c$ has also become noticeable, indicating that even manual grinding of the specimen tends to increase the magnitude of the out-of-phase octahedral tilt of the rhombohedral phase. Thus, similar to the poling field, mechanical impact also leads to phase separation of the critical cubiclike phase. However, the transformation does not seem to be complete to its possible limit by mere mechanical impact since the intensity of the superlattice peak is not as pronounced in the unpoled-crushed pattern as in the poled-crushed pattern. In a separate experiment, we found that the diffraction pattern obtained from the surface of a poled pellet of $x = 0.065$ exhibited similar splitting of the peaks as observed for the poled-crushed pattern. Since the pellet was not subjected to mechanical impact, the phase separation was effected by the poling field. This proves that the phase separation in the sufficiently poled-crushed specimen is primarily due to the effect of electric field and the impact-induced features in the diffraction pattern are of secondary importance, if any.

Figure 11(a) shows the evolution of the x-ray powder diffraction profiles of $x = 0.065$ as a function of varying poling fields. It may be noted that at low poling fields, the features in the diffraction pattern would be dominated by mechanical impact-induced structural changes. Hence, in this plot, even for the zero poling field (unpoled-crushed specimen), the rhombohedral fraction is shown to exist (~60%). The field-induced structural changes start dominating the system above the coercive field. Rietveld analysis of the poled-crushed patterns at different poling fields suggested a decrease in the rhombohedral phase with increasing field [Fig. 11(b)]. It attained a minimum value of ~30% above 20 kV/cm. It must be emphasized that for low-poling field-crushed specimens,

TABLE II. Refined structural parameter of the poled-crushed specimen of $x = 0.065$. Refinement was carried out with $P4mm + R3c$ structural model. The isotropic displacement parameter B is in Å^2. The (0)s against parameters indicate that these parameters were not refined.

$x = 0.065$ (Poled)		Tetragonal ($P4mm$) phase				Rhombohedral ($R3c$) phase			
a,b,c (Å)		3.8929(2)	3.8929(2)	3.9383(3)		5.5014(2)	5.5014(2)	13.6030(7)	
Na/Bi/Ba	x,y,z B	0.0000	0.0000	0.0000	1(0)	0.0000	0.0000	0.2840(17)	1.5(2)
Ti	x,y,z B	0.50	0.50	0.5442(26)	1(0)	0.0000	0.0000	0.0176(22)	1(0)
O1	x,y,z B	0.50	0.50	0.0898(56)	1(0)	0.1287(25)	0.3464(35)	0.08333	1(0)
O2	x,y,z B	0.5	0.0000	0.6090(36)	1(0)				
Phase fraction		73%				27%			

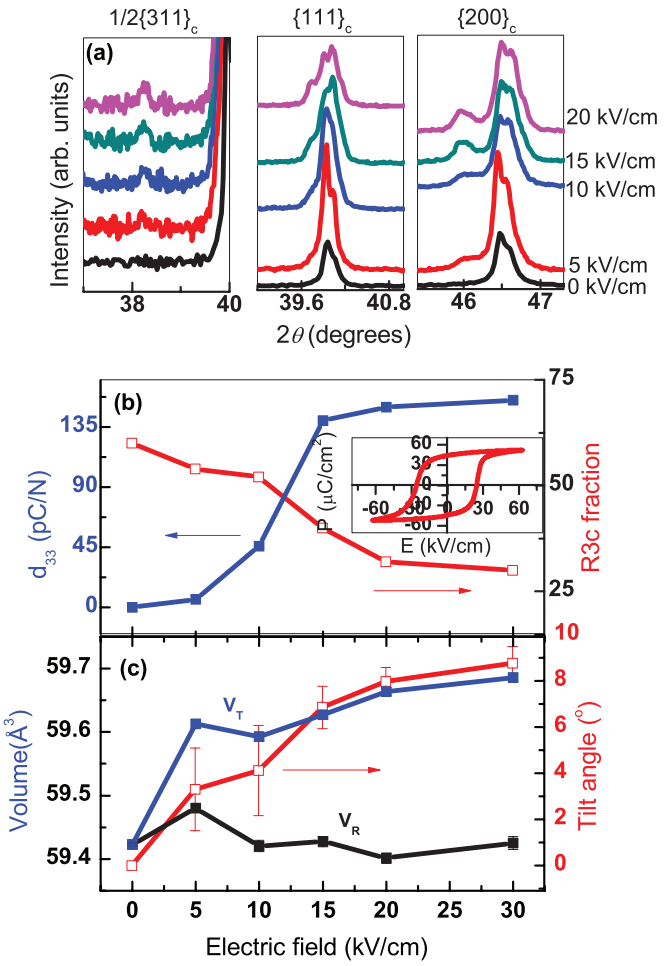

FIG. 11. (Color online) (a) XRD plots of $x = 0.065$ electrically poled at different electric fields. (b) Variation of volume fraction of $R3c$ and longitudinal piezoelectric coefficient with poling field of $x = 0.065$. The inset shows polarization-electric field hysteresis loop of this composition. (c) Poling field dependence of the unit cell volume of the phase-separated tetragonal and rhombohedral phases and octahedral tilt angle.

the system would exhibit a combined effect of mechanical impact as well electric field-induced changes, and hence it may not be appropriate to attribute the variation in the absolute value of the phase fractions entirely to the poling field as shown in Fig. 11(b). However, it is interesting that the longitudinal piezoelectric coefficient, d_{33} for $x = 0.065$, saturates at a field of 15 kV/cm, which is significantly lower than the field (~25 kV/cm) required to saturate the d_{33} for the precritical composition $x = 0.05$. The significant lowering of the critical poling field for obtaining maximum possible d_{33} can be attributed to the onset of composition-induced criticality in the system. The rhombohedral tilt angle increases from nearly 0 to ~9° with increasing poling field, Fig. 10(c). This variation is also consistent with the development of the rhombohedral strain with increasing poling field, as manifested by the increased splitting in the doublet of $\{111\}_c$ profile.

E. Dielectric behavior and coherence length of the octahedral tilt

1. Field-induced irreversible relaxor to normal ferroelectric transformation

Figure 12 shows the temperature dependence of real $\varepsilon'(T)$ and imaginary $\varepsilon''(T)$ part of dielectric permittivity of unpoled $x = 0.06$. The real part shows a broad peak at 270 °C. At low measuring frequencies (e.g., 1 kHZ), a shoulder becomes noticeable in $\varepsilon'(T)$ at ~145 °C. The imaginary part exhibits considerable temperature-dependent dielectric relaxation near this temperature [Fig. 12(a)]. The increasing value of the dielectric loss permittivity (imaginary part) maximum temperature with increasing frequency is akin to systems exhibiting relaxor ferroelectricity.[44,45] The Vogel-Fulcher relation

$$f = f_0 \exp\left[\frac{-E_a}{k(T_m - T_{VF})}\right]$$

was used to estimate the relaxational freezing temperature of the polar clusters.[44,45] E_a and f are the activation energy and frequency at which ε'' shows the maximum, respectively. The inset of Fig. 12(a) shows the result of Vogel-Fulcher fitting to dielectric data of $\varepsilon''(T)$. The best fit was obtained with $T_{VF} = 108$ °C, $f_0 = 1.0 \times 10^6$ Hz, and $E_a = 6.5$ meV. These values are comparable to that reported earlier by Ranjan and Dwivedi[11] for the cubiclike critical compositions of this system. In contrast to the unpoled specimens, the temperature variation of the dielectric permittivity of the poled specimens, shown in Fig. 12(b), reveals a sharp maximum in the real and imaginary part of dielectric permittivity. For example, a sharp anomaly occurs at 108 °C, and the frequency dispersion in the ε' and ε'' below this temperature is insignificant. Interestingly, however, there is a sudden increase in the frequency dispersion just after this temperature. Thus, this temperature corresponds to a normal ferroelectric-relaxor ferroelectric transition temperature (T_{F-R}). Most remarkably, this temperature coincides with the Vogel-Fulcher freezing temperature (T_{VF}) obtained from the $\varepsilon''(T)$ of the unpoled specimen. Above T_{F-R}, the dielectric behavior of the unpoled and the poled specimen are qualitatively similar. In the unpoled state, the continuity of considerable dielectric dispersion well below the dipolar freezing temperature (T_{VF}) suggests that the polar nanoregions could not grow and coalesce to yield a normal ferroelectric state. The system rather settles in a dipolar glass state.[45] However, application of poling field to the frozen dipolar configuration helps the system achieve long-range polar order and irreversibly transform the dipolar glass state to a normal ferroelectric state.

2. Field-induced enhancement of the coherence length of the octahedral tilt

Figures 13(a) and 13(b) show magnified plots of the neutron diffraction patterns of annealed and poled-crushed specimen of $x = 0.0675$, respectively, in a limited 2θ region. In conformity with the XRD study shown in Fig. 6(b), where poling led to a sudden visibility of the superlattice reflection corresponding to the out-of-phase octahedral tilt, the neutron diffraction pattern

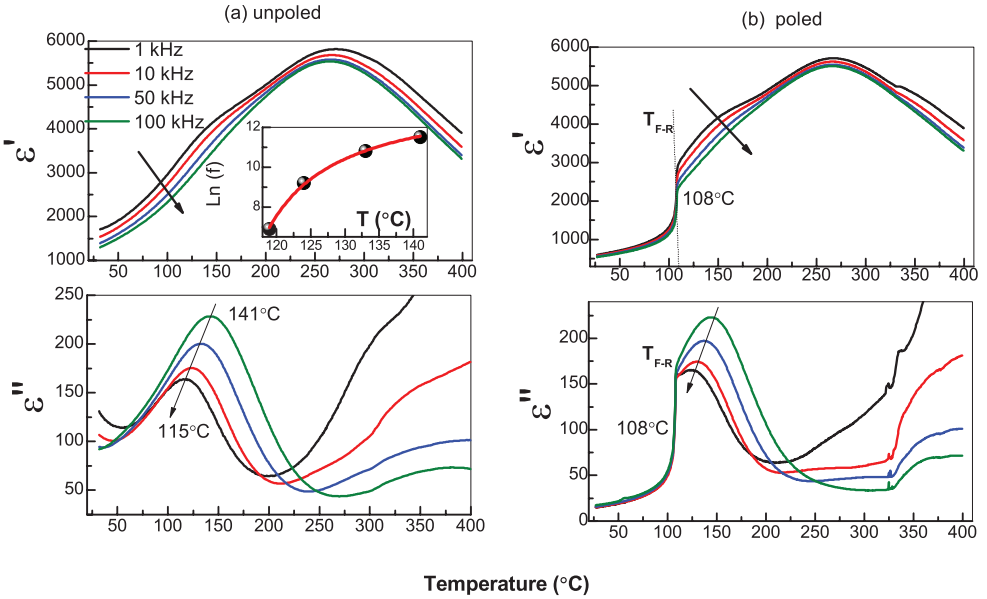

FIG. 12. (Color online) Temperature variation of the real (ε') and the imaginary part (ε'') of the relative permittivity of $x = 0.06$ at different frequencies for (a) unpoled and (b) poled specimens. The arrows show increasing frequency.

manifests this phenomenon more vividly. The intensity of the $\frac{1}{2}\{311\}_c$ superlattice reflection, which is very weak in the annealed pattern [Fig. 13(a)], increases manifold in the poled pattern [Fig. 13(b)]. Also new superlattice reflections, $\frac{1}{2}\{331\}_c$ and $1/2\{511\}_c$, which were not visible in the annealed pattern become very prominent in the poled pattern. Concomitantly, the intensity of the $\frac{1}{2}\{310\}_c$ and the neighboring unindexed superlattice peak (∗) decreased in the poled pattern. This observation is of significance. Since the poling field affects the intensity of the unindexed peak, it implies that the unindexed superlattice peak has its origin in the same structure, which also gives the $\frac{1}{2}\{310\}_c$ peak. A correct structural model of the tetragonal phase must explain not only the intensity of the $\frac{1}{2}\{310\}_c$ superlattice peak but also the extra superlattice peak adjacent to the $\frac{1}{2}\{310\}_c$. It may be noted that the main Bragg peaks in the poled pattern exhibit broadening and splitting [see the inset of Fig. 13(b)]. As discussed above in Sec. III D, this is due to the development of significant lattice distortion in the rhombohedral and tetragonal phases.

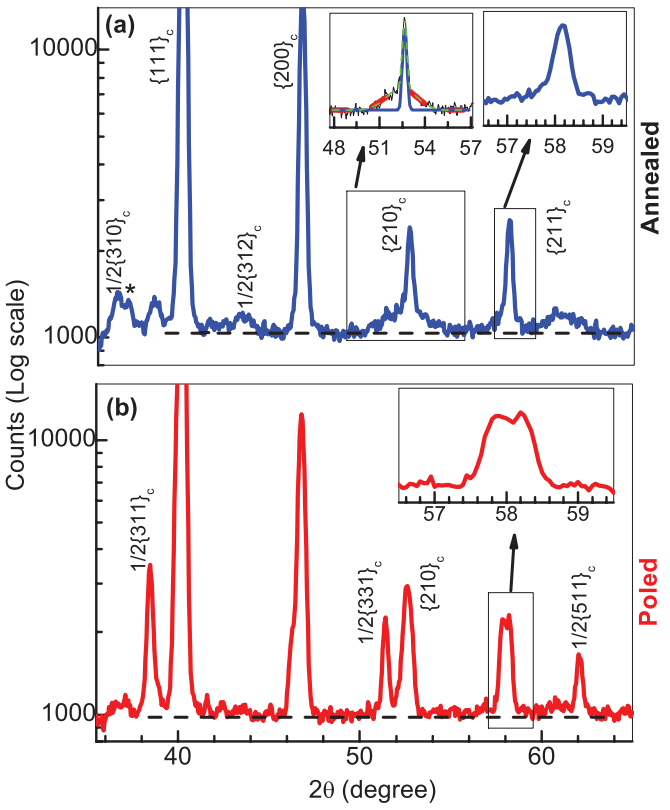

FIG. 13. (Color online) Neutron powder diffraction patterns of $x = 0.0675$ (a) annealed specimen and (b) poled-crushed specimens. The left inset in (a) shows fitting of the broad superlattice hump and the superposed pseudocubic $\{210\}_c$ peak.

Another significant observation that is of great importance is the wavy nature of the background in the annealed pattern and it becoming almost flat in the poled pattern. This wavy background is therefore due to extra scattering away from the main peaks coming from the specimen itself and is not an experimental artifact. For example, on either side of the $\{210\}_c$, the tail falls gradually. The main Bragg peak $\{210\}_c$ rather appears to be sitting on a weak broad hump spanning 50–55° in 2θ. Similarly, a weak and broad peak is seen just after the $\{211\}_c$ in the annealed pattern. In the poled specimen, the spread of the peak vanish to give way to sharp and prominently visible new *ooo* superlattice reflections. This is direct proof of the fact that the poling field has considerably increased the coherence length of the out-of-phase octahedral tilt irreversibly. Considering the width of the superlattice reflections in the poled pattern displays no finite correlation length effect, the excess width of the corresponding weak peaks in the annealed pattern can be used to estimate the spatial correlation of the octahedral tilt in the annealed specimen.

The coherence length of the out-of-phase octahedral tilt in the annealed specimen was calculated from the FWHM of the broad hump on $\{210\}_c$, which is shown in inset of Fig. 13(a), and was found to be ∼50 Å. A similar value was obtained with the broad peak on the right of $\{211\}_c$.

IV. DISCUSSION

A. Structure piezoelectric-response correlation

In general, high piezoelectric response in ferroelectric systems has been associated with the occurrence of MPB, which is characterized by the coexistence of two structurally different ferroelectric phases in the equilibrium state. The prototype systems that represent this situation are $[Pb(Zn_{1/3}Nb_{2/3})O_3]_{1-x}$ $[PbTiO_3]_x$ (PZN-PT), $[Pb(Mg_{1/3}Nb_{2/3})O_3]_{1-x}$ $[PbTiO_3]_x$ (PMN-PT), and $Pb(Zr_xTi_{1-x})O_3$ (PZT).[20–25,46,47] The MPB compositions in these systems exhibit the coexistence of rhombohedral/monoclinic and tetragonal phases at room temperature. The low-symmetry monoclinic phase offers a continuous polarization rotation pathway. On application of the external electric field, the polarization vector takes the low-energy path from one high-symmetry direction to another (say $[001]_c$ to $[111]_c$), thereby exhibiting a high piezoelectric response.[30] Apart from this intrinsic contribution, extrinsic contribution to the piezoresponse comes from the motion of interphase and domain boundaries.[48,49] While the occurrence of the monoclinic phase has been experimentally established for the MPB compositions of lead-based systems,[20,24,25] the dominant mechanism leading to enhanced piezoresponse is still unclear in NBT-BT. Although Cordero *et al.*[5] have suggested the possibility of local monoclinic distortion with short correlation lengths to explain the diffuse temperature variation of elastic compliance, so far there has been no report ascertaining the evidence of the monoclinic phase for the critical compositions of NBT-BT. In fact, such local monoclinic distortions have also been proposed for pure NBT,[50,51] which later were found to exist as a Cc phase.[26,27,32] However, as shown in Fig. 2(b), the presence of the Cc phase does not ensure higher piezoelectric response for $x = 0.05$. The highest d_{33} is rather obtained for the compositions exhibiting a cubiclike structure. At first, it may appear counterintuitive to suggest that a cubiclike structure should show as large a piezoelectric response as the adjacent MPB composition $x = 0.07$. The answer is to be found in the structure of the poled specimen. Since piezoelectric response is measured on poled pellets and the poled specimen no longer exhibits a cubiclike structure, but the MPB-like structure, it becomes understandable why the composition that exhibits a cubiclike structure in the equilibrium state gives a large piezoelectric response. The equilibrium MPB composition $x = 0.07$, on the other hand, retains its MPB character with a slight decrease in the rhombohedral/cubiclike phase fraction after poling and hence gives a comparable piezoelectric response as the equilibrium cubiclike compositions. On the contrary, the precritical compositions ($x \leqslant 0.05$) transform from a two-phase $Cc + R3c$ to a single-phase $R3c$ after poling. The presence of the monoclinic phase in the equilibrium state of the precritical compositions does not contribute to the piezoresponse simply because this phase ceases to exist after poling. Had the system retained the $Cc + R3c$ phase coexistence in the poled state, one would have anticipated a better piezoelectric response in NBT as well. Compared to a two-phase state, the single-phase ($R3c$) state in the poled state of NBT is not good for enhanced piezoelectric response because it can neither afford intrinsic polarization rotation nor does the system in the pure $R3c$ phase have a large number of active interphase boundaries to give extrinsic contribution to the overall piezoresponse. From the above, it is obvious that the monoclinic phase observed in the precritical compositions of the NBT-BT is not critically active as in the MPB compositions of PZT or PMN-PT. The reason may be found in the way the coexistence of ferroelectric phases appears at room temperature in PZT and in NBT. While the formation of a monoclinic phase in lead-based piezoelectrics is intimately linked to the composition-induced ferroelectric-ferroelectric instability, the monoclinic phase seems to be "passive" in NBT. For NBT, it may be plausible to argue that the monoclinic phase might have appeared from one of the paraelectric structures. A likely scenario is that the intermediate orthorhombic, *Pbnm* (Refs. 52 and 53), paraelectric phase could have transformed to the ferroelectric Cc phase on cooling, and the $R3c$ phase would have come from the $P4bm$ phase. From this analysis, it becomes obvious that as far as the understanding of the structure-property correlations in NBT-derived piezoelectric systems is concerned, what matters is not the structure of the system in the equilibrium state but rather that the irreversibly transformed structures under the application of the poling field would determine the piezoelectric response of the system. If the system is able to induce phase coexistence as in $0.06 \leqslant x \leqslant 0.0675$, or retain the phase coexistence as in $x = 0.07$, the system would exhibit a higher piezoelectric response.

B. Equilibrium structures and dielectric relaxation

The cubiclike critical compositions of NBT-BT have been suggested to be more like a relaxor ferroelectric than a normal ferroelectric. This was based on the close similarity in the frequency dispersion exhibited by these compositions and those exhibited by the La-modified PZT-based relaxor ferroelectrics.[19] In fact, from the temperature-dependent dielectric behavior, the parent compound NBT itself has traditionally been called as a relaxor ferroelectric[54,55] instead of a normal ferroelectric. The three compositions $x = 0.05$ (the precritical composition), $x = 0.06$ (cubiclike critical composition), and $x = 0.07$ (the MPB critical composition) were found to exhibit significant dielectric relaxation. It may, therefore, not be an appropriate approach to attempt to establish a one-to-one correlation between the gross structural features of NBT-BT in the different composition range with its dielectric behavior. In general, the relaxor ferroelectric behavior of a ferroelectric system is associated with structural disorder that prevents development of long-range polar ordering. Experimentally, an indirect way of capturing structural disorder is through measuring the excess width of the Bragg profiles in a diffraction pattern. The excess width of the profiles can arise due to random lattice strain associated with the structural disorder. Interestingly however, the FWHM of the Bragg peaks of $x = 0.06$ is comparable to the instrumental FWHM (0.08°), suggesting almost no noticeable random lattice strain

in the cubiclike compositions. We may note that our attempt to find a noncubic distortion by fitting the XRD pattern of $x = 0.06$ with the rhombohedral structure model failed as refinement cycles were oscillatory and did not converge. The cubic model, on the other hand, easily fitted the pattern in a few cycles. Since the intensity of the Bragg peaks in the neutron diffraction pattern is very sensitive to oxygen coordinates (as compared to x-rays) and also because the neutron diffraction pattern has a significantly larger number of Bragg peaks to fit to, it was expected that a wrong structural model would lead to a noticeable mismatch between the observed and fitted patterns, at least for the peaks at high 2θ angles. We therefore fitted the neutron diffraction pattern with cubic and rhombohedral models and found the quality of fit to be equally good with both ($\chi^2{}_{Pm3m} = 4.38$ and $\chi^2{}_{R3c} = 4.23$). The XRD and the neutron diffraction patterns therefore clearly suggest that the average structure of $0.06 \leqslant x \leqslant 0.0675$ must indeed be very close to the true cubic structure. This is a bit puzzling since the rhombohedral and the tetragonal structures in the phase-separated state exhibit noticeable rhombohedral distortion ($60 - \alpha_{\rm rh} = 0.36^\circ$) and tetragonal distortion (c-a = 0.045 Å). If these distortions are considered to represent the natural (spontaneous) distortions of these structures, as in the MPB compositions, then it would imply that the cubiclike phase must have accommodated significant strain energy. Note that the intensity of the Bragg peaks in the XRD pattern is primarily determined by the sublattice of the high Z cations (Na/Bi and Ti) due to comparatively low scattering of x-rays by oxygen. In view of this, the absence of any measurable strain (excess FWHM) would imply that the cations are arranged in a perfect cubic array. In what way, then, does the cubiclike structure accommodate the spontaneous strain energy corresponding to the two structures? It appears that instead of inducing random elastic strain in the lattice, the system prefers to use the excess energy in creating random faults in the otherwise orderly $a^-a^-a^-$ octahedral tilt configuration. As a result, the coherence length of the $a^-a^-a^-$ octahedral tilt has considerably decreased (~50 Å). The faulted region consists of a complex octahedral tilt, not like the tetragonal $P4bm$ structure corresponding to the simple $a^0a^0c^+$ tilt.

The electric dipole formation in perovskites is associated with the relative displacement of the oxygen sublattice with respect to the cation sublattice. Assuming that the main contribution to the overall polarization comes from the relative displacement of the oxygen sublattice with respect to the Ti-sublattice, the coherence length of the $a^-a^-a^-$ tilt can be considered to be intimately linked with the coherence length of the dipolar ordering in the system. At room temperature, which is well below the freezing temperature of the polar nanoregions, the system remains in the dipolar glass state due to the finite coherence length of the out-of-phase octahedral tilt. However, since polarization couples directly with the external electric field, the poling field would try to align the frozen polar nanoregions in the direction of the field and make them grow by merging the neighboring polar nanoregions. The poling field therefore transforms the dipolar glassy state to a normal ferroelectric state at room temperature. By virtue of the strong coupling of the octahedral tilt with the polarization, the field-induced irreversible development of the ferroelectric state concomitantly increases the coherence length of the $a^-a^-a^-$ octahedral tilt. The neutron diffraction study clearly suggests that the development of the long-range ordered polar state occurs together with not only the enhancement of the coherence length of the $a^-a^-a^-$ tilt configuration but also with the considerable increase in the magnitude of the out-of-phase octahedral tilt angle. At the same time, the reduction in the intensity of the $\frac{1}{2}\{310\}_c$ and the accompanying unindexed superlattice peak indicate suppression of complex tilt configuration in favor of the $a^-a^-a^-$ octahedral tilt configuration. As evident from the neutron diffraction pattern of the poled specimens, this complex tilt configuration still survives after poling, although with a reduced magnitude.

V. CONCLUSION

In this paper we report a comprehensive structural study of $(1-x)$NBT-(x)BT series close to its MPB as a function of composition, temperature, electric field, as well as mechanical impact by x-ray and neutron powder diffraction and Raman spectroscopy. Although the XRD study of the equilibrium state (annealed specimens) revealed three distinct composition ranges, characteristic of three different structural states: $Cc + R3c$ phase coexistence for $x \leqslant 0.05$, cubiclike for $0.06 \leqslant x \leqslant 0.0675$, and MPB-like for $0.07 \leqslant x \leqslant 0.10$, Raman spectra revealed that symmetrywise the cubiclike and the MPB compositions are identical. The ambiguity was resolved by a neutron diffraction study that showed that irrespective of the type of lattice distortion present in the system, all exhibit the same set of superlattice reflections. The neutron diffraction study revealed a very short coherence length (~50 Å) of the out-of-phase octahedral tilt in the equilibrium state of the cubiclike critical compositions. The system exhibits relaxor ferroelectric behavior in this state. The short coherence length of the out-of-phase octahedral tilt prevents development of long-range polar ordering, i.e., the normal ferroelectric state below the dipolar freezing temperature. The poling field not only helps bring about a normal ferroelectric state, but by virtue of the strong coupling of the polarization with the out-of-phase octahedral tilt, it considerably enhances the coherence length of the $a^-a^-a^-$ tilt. The comparable piezoelectric response of the cubiclike compositions with those of the MPB compositions can be understood from the poling field-induced phase separation of the cubiclike compositions, making them MPB-like. This study suggests that the correct approach towards understanding the structure-property correlations in the NBT-BT system should be guided primarily by the irreversible structural changes that accompany electric poling of the specimen and should not be based on the structures in the equilibrium state.

ACKNOWLEDGMENTS

R.R. gratefully acknowledges financial assistance from Department of Science and Technology, Government of India, and the Council of Scientific and Industrial Research, India.

*rajeev@materials.iisc.ernet.in

[1] B. Jaffe, W. R. Cook, and H. Jaffe, *Piezoelectric Ceramics* (Academic Press, London, 1971).
[2] T. Takenaka, K. Maruyama, and K. Sakata, Jpn. J. Appl. Phys., Part 1 **30**, 2236 (1991).
[3] C. Ma and X. Tan, Solid State Commun. **150**, 1497 (2010).
[4] B. W. Eerd, D. Damjanovic, N. Klein, N. Setter, and J. Trodahl, Phys. Rev. B **82**, 104112 (2010).
[5] F. Cordero, F. Craciun, F. Trequattrini, E. Mercadelli, and C. Galassi, Phys. Rev. B **81**, 144124 (2010).
[6] W. Jo, J. E. Daniels, J. L. Jones, X. Tan, P. A. Thomas, D. Damjanovic, and J. Rödel, J. Appl. Phys. **109**, 014110 (2011).
[7] Y. S. Sung, J. M. Kim, J. H. Cho, T. K. Song, M. H. Kim, and T. G. Park, Appl. Phys. Lett. **96**, 202901 (2010).
[8] J. Yao, L. Yan, W. Ge, L. Luo, J. Li, and D. Viehland, Phys. Rev. B **83**, 054107 (2011).
[9] G. Picht, J. Töpfer, and E. Henning, J. Eur. Ceram. Soc. **30**, 3445 (2010).
[10] C. Ma, X. Tan, E. Dul'kin, and M. Roth, J. Appl. Phys. **108**, 104105 (2010).
[11] R. Ranjan and A. Dviwedi, Solid State Commun. **135**, 394 (2005).
[12] M. Chen, Q. Xu, B. H. Kim, B. K. Ahn, J. H. Ko, W. J. Kang, and O. J. Nam, J. Eur. Ceram. Soc. **28**, 843 (2008).
[13] Q. Xu, S. Chen, W. Chen, S. Wu, J. Zhou, H. Sun, and Y. Li, Mater. Chem. Phys. **90**, 111 (2005).
[14] J. E. Daniels, W. Jo, J. Rödel, and J. L. Jones, Appl. Phys. Lett. **95**, 032904 (2009).
[15] H. Simons, J. Daniels, W. Jo, R. Dittmer, and A. Studer, Appl. Phys. Lett. **98**, 082901 (2011).
[16] C. Ma and X. Tan, J. Am. Ceram. Soc. **94**, 4040 (2011).
[17] Y. M. Chiang, G. W. Farrey, and A. N. Soukhojak, Appl. Phys. Lett. **73**, 3683 (1998).
[18] W. Ge, H. Cao, J. Li, D. Viehland, and Q. Zhang, Appl. Phys. Lett. **95**, 162903 (2009).
[19] W. Jo, S. Schaab, E. Sapper, L. A. Schmitt, H. J. Kleebe, A. J. Bell, and J. Rödel, J. Appl. Phys. **110**, 074106 (2011).
[20] R. Guo, L. E. Cross, S.-E. Park, B. Noheda, D. E. Cox, and G. Shirane, Phys. Rev. Lett. **84**, 5423 (2000).
[21] S. E. Park and T. R. Shrout, J. Appl. Phys. **82**, 1804 (1997).
[22] B. Noheda, D. E. Cox, and G. Shirane, Phys. Rev. B **66**, 054104 (2002).
[23] B. Noheda, D. E. Cox, G. Shirane, J. A. Gonzalo, L. E. Cross, and S. E. Park, Appl. Phys. Lett. **74**, 2059 (1999).
[24] B. Noheda, D. E. Cox, G. Shirane, S. E. Park, L. E. Cross, and Z. Zhong, Phys. Rev. Lett. **86**, 3891 (2001).
[25] D. Pandey, A. K. Singh, R. Ranjan, and Ragini, Ferroelectrics **325**, 35 (2005).
[26] S. Gorfman and P. A. Thomas, J. Appl. Crystallogr. **43**, 1409 (2010).
[27] E. Aksel, J. S. Forrester, J. L. Jones, P. A. Thomas, K. Page, and M. R. Suchomel, Appl. Phys. Lett. **98**, 152901 (2011).
[28] T. M. Usher, J. S. Forrester, C. R. D. Cruz, and J. L. Jones, Appl. Phys. Lett. **101**, 152906 (2012).
[29] E. Aksel, J. S. Forrester, B. Kowlski, J. L. Jones, and P. A. Thomas, Appl. Phys. Lett. **99**, 222901 (2011).
[30] H. Fu and R. Cohen, Nature (London) **403**, 281 (2000).
[31] L. Bellaiche, A. García, and D. Vanderbilt, Phys. Rev. B **64**, 060103(R) (2001).
[32] B. N. Rao and R. Ranjan, Phys. Rev. B **86**, 134103 (2012).
[33] J. Rodrigues-Carvajal, *FULLPROF. A Rietveld Refinement and Pattern Matching Analysis Program* (Laboratoire Leon Brillouin, CEA-CNRS, France, 2000).
[34] J. Kreisel, A. M. Glazer, G. Jones, P. A. Thomas, L. Abello, and G. Lucazeau, J. Phys.: Condens. Matter **12**, 3267 (2000).
[35] J. Kreisel, A. M. Glazer, P. Bouvier, and G. Lucazeau, Phys. Rev. B **63**, 174106 (2001).
[36] V. Dorcet and G. Trolliard, Acta Mater. **56**, 1753 (2008).
[37] C. Ma, H. Guo, S. P. Beckman, and X. Tan, Phys. Rev. Lett. **109**, 107602 (2012).
[38] J. Yao, N. Monsegue, M. Murayama, W. Leng, and W. T. Reynolds, Appl. Phys. Lett. **100**, 012901 (2012).
[39] R. D. Shannon, Acta Crystallogr. Sec. A **32**, 751 (1976).
[40] A. M. Glazer, Acta Crystallogr. Sec. B **28**, 3384 (1972).
[41] A. M. Glazer, Acta Crystallogr. Sec. A **31**, 756 (1975).
[42] G. O. Jones and P. A. Thomas, Acta Crystallogr. Sec. B **58**, 168 (2002).
[43] G. O. Jones and P. A. Thomas, Acta Crystallogr. Sec. B **56**, 426 (2000).
[44] G. A. Samara, J. Phys.: Condens. Matter **15**, R367 (2003).
[45] L. E. Cross, Ferroelectrics **76**, 241 (1987).
[46] J. Kuwata, K. Uchino, and S. Nomura, Ferroelectrics **37**, 579 (1981).
[47] T. Shrout, Z. P. Chang, N. Kim, and S. Markgraf, Ferroelectr., Lett. Sect. **12**, 63 (1990).
[48] D. Damjanovic, IEEE Trans. Ultrason. Ferroelectr. Freq. Control **56**, 1574 (2009).
[49] D. Damjanovic, Appl. Phys. Lett. **97**, 062906 (2010).
[50] J. Frantti, Y. Fujioka, and R. M. Nieminen, J. Phys.: Condens. Matter **20**, 472203 (2008).
[51] E. P. Smirnova, A. V. Sotnikov, O. E. Kvyatkovskii, M. Weihnacht, and V. V. Lemanov, J. Appl. Phys. **101**, 084117 (2007).
[52] V. Dorcet, G. Trolliard, and P. Boullay, Chem. Mater. **20**, 5061 (2008).
[53] G. Trolliard and V. Dorcet, Chem. Mater. **20**, 5074 (2008).
[54] S. B. Vakhrushev, V. A. Isupov, B. E. Kvyatlovsky, N. M. Okuneva, I. P. Pronin, G. A. Smolensky, and P. P. Syrnikov, Ferroelectrics **63**, 153 (1985).
[55] J. Suchanicz and J. Kwapulinski, Ferroelectrics **165**, 249 (1995).